

## Repeatable calibration of Hounsfield units to mineral density and effect of scanning medium

Meghan Crookshank<sup>1,2</sup>, Heidi-Lynn Ploeg<sup>2,3</sup>, Randy Ellis<sup>2,4</sup>  
and Norma J. MacIntyre<sup>2,5</sup>

<sup>1</sup>Biomedical Engineering, University of Toronto, Toronto, ON M5B 1W8, Canada

<sup>2</sup>Human Mobility Research Centre, Queen's University & Kingston General Hospital, Kingston, ON K7L 3N6, Canada

<sup>3</sup>Mechanical Engineering, University of Wisconsin, Madison, WI 53706, USA

<sup>4</sup>School of Computing, Queen's University, Kingston, ON K7L 3N6, Canada

<sup>5</sup>School of Rehabilitation Science, McMaster University, Hamilton, ON L8S 1C7, Canada

(Received July 13, 2012, Revised February 12, 2013, Accepted February 13, 2013)

**Abstract.** Computed tomography (CT) is being utilized in orthopaedics and related research to estimate bone strength. These applications benefit from calibration of Hounsfield units to mineral density typical of long bone, up to 1750mg/cm<sup>3</sup>. This study describes a method for establishing repeatable calibration of Hounsfield units to density, and determines the effects of imaging medium on calibration accuracy. Four hydroxyapatite standards were imaged in air on 7 occasions over 19 weeks using a helical multi-slice CT scanner. Each standard was scanned 5 times in different media: porcine soft tissue, water, and air. Calibrated densities were highly repeatable (CV<3.5%). No difference in density was observed between water and soft tissue conditions (p>0.08). This work provides a model for determining repeatable scanner-specific density calibration, demonstrates that the linear relationship between Hounsfield units and density extends to values typical of cortical bone, and supports the practice of imaging calibration standards in an environment similar to that of the target bone.

**Keywords:** computed tomography; reliability; cortical bone; trabecular bone; bone density

### 1. Introduction

Computed tomography (CT) is increasingly being utilized in orthopaedic research and clinical practice to estimate bone strength. It is a standard method for the generation of finite element (FE) analyses of long bones. CT-based FE models have been developed to perform quantitative simulation of failure loads in a variety of anatomical locations as well as implant stability (Reggiani *et al.* 2006, Bessho *et al.* 2007, Pietruszczak *et al.* 2007, Au *et al.* 2007, Gong *et al.* 2012). Additionally, CT, particularly at higher resolution, is being investigated for roles in diagnosing osteoporosis, assessing fracture healing, classifying fracture risk and surgical planning (Kazakia *et al.* 2006, Bouxsein 2008, Kalpakcioglu *et al.* 2008). For many of these applications, the CT numbers, expressed in Hounsfield units (HU) of a particular scan are converted to mineral

---

\*Corresponding author, Associate Professor, E-mail: [macint@mcmaster.ca](mailto:macint@mcmaster.ca)

density to provide an estimation of bone strength and, for long bones in particular, cortical bone density is a very important determinant.

Methods have been developed for converting HU to mineral density values using density standards that simulate the apparent density of trabecular bone (Genant *et al.* 1982, Kalender and Suess 1987, Steiger *et al.* 1990). In some methods, aqueous solutions of potassium phosphate represent mineral densities from 0 to 400 mg/mL (Genant *et al.* 1982); in other methods, homogeneous hydroxyapatite equivalent material with densities of 50, 100, and 200 mg/cm<sup>3</sup> are used (Brailon 2002). A linear relationship exists between HU and reference standards falling within this range of densities (Genant *et al.* 1982, Kalender and Suess 1987, Steiger *et al.* 1990, Brailon 2002) and as few as two standards (0 and 200 mg/cm<sup>3</sup>) are sufficient for accurate calibration (Kalender and Suess 1987). To date, however, it is unclear whether the same linear relationship which exists between HU and density within the range typical of trabecular bone extends to the higher densities typical of cortical bone.

When constructing CT-based estimates of bone strength, selection of the correct medium in which to scan bones and standards is required. Since beam hardening is caused by X-ray attenuation by the various materials through which the beam passes, it follows that the medium in which a sample is imaged will have an effect on the resulting HU (Araki and Okano 2011, Brooks and DiChiro 1976, Van Gompel *et al.* 2011). As such, it is important that the calibration standards be imaged in an environment similar to the specific region of interest in the patient in CT-based assessment of fracture healing, diagnosis of osteoporosis and surgical planning. Based on theory rather than empirical evidence, it is generally accepted that water is a good simulation for soft tissue, as the attenuation characteristics of muscle and water are similar. Many researchers use volumes of water to approximate the X-ray attenuation due to soft tissue when scanning specimens *ex vivo* (Bessho *et al.* 2007, Schileo *et al.* 2008, Unnikrishnan and Morgan 2011). Not all researchers state whether the bone specimens or the calibration standards were surrounded by a medium and the reader is left to assume that the samples were surrounded by air.

The objectives of this study were to 1) illustrate an experimental approach for establishing repeatable scanner-specific calibration of CT number to density values appropriate for trabecular and cortical bone, and 2) determine the effect of imaging medium on calibration accuracy.

## 2. Methods

### 2.1 Calibration standards

Four hydroxyapatite standards (CIRS Inc, Norfolk, VA) were selected to encompass the apparent densities typical of human trabecular and cortical bone (Curry 1988). The densities of the four standards were 100, 400, 1000, and 1750 mg/cm<sup>3</sup>, which represent milligrams per cubic centimeter equivalents of hydroxyapatite. The two standards having the highest densities were manufactured as plugs within a water-equivalent material representative of apparent densities of human cortical bone (part numbers 06217 and 06221).

### 2.2 Imaging protocol

All scans were performed using a helical multi-slice CT scanner (Lightspeed Plus, General Electric Medical Systems, Milwaukee, WI) and the following imaging parameters: 120 kVp,

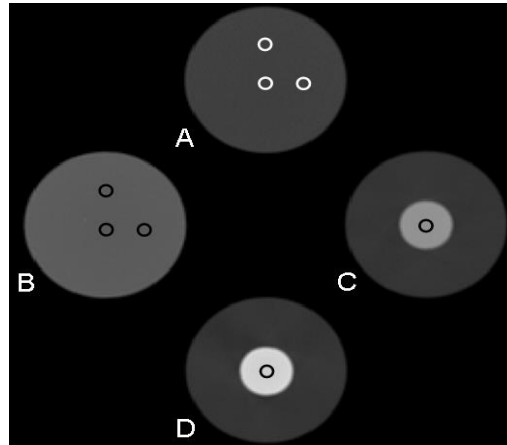


Fig. 1 Locations of the regions of interest identified within each standard at 25%, 50% and 75% of the total length: (a) 100 mg/cm<sup>3</sup> standard, (b) 400 mg/cm<sup>3</sup> standard, (c) 1000 mg/cm<sup>3</sup> standard and (d) 1750 mg/cm<sup>3</sup> standard

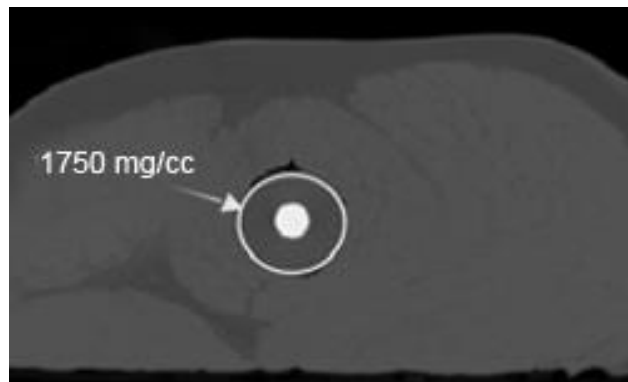


Fig. 2 Each standard was inserted into a cross-shaped incision in the center of the porcine soft tissue

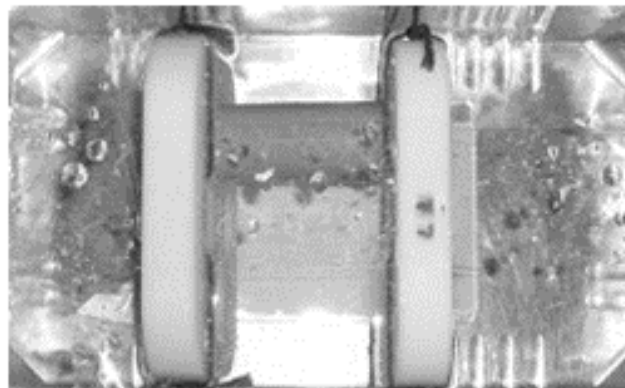


Fig. 3 The custom holder is used to secure each end of the standards in the center of a water-filled container. One standard is shown here in the assigned position within the rhombus-shaped configuration

120 mAs, 2.5 mm slice thickness, 1.25 mm slice spacing.

To determine the repeatability of the method, the standards were imaged in air in a rhombus-shaped configuration, as illustrated in Fig. 1, in seven replicate scans over a 19-week period. To compare the effect of scanning media on density calibration, each standard was suspended in three different media: porcine thigh soft tissue, tap water, and air, and five replicate scans were acquired. Densities representative of human soft tissue were approximated using fresh-frozen porcine soft tissue, stored at  $-40^{\circ}\text{C}$  and thawed at room temperature for 24 hours prior to imaging. The standards were inserted into a cross-shaped incision in the center of the soft tissue as illustrated in Fig. 2. For soft tissue and water, cross-sectional area of the media was constant ( $286\text{ cm}^2$ ). A custom holder was used to secure both ends of each standard such that it was centered within the volume of water and suspended in air. The standards and holder were placed in a container positioned on a low-density foam pad to center the standard in the scan-field and to provide a contrast between the standard and the aluminum scan-bed as shown in Fig. 3.

### *2.3 Image analysis*

Average HU for each standard were determined for circular ROIs ( $10\text{ mm}^2$ ) identified in the image slice located at 25%, 50% and 75% the total length of the standard using image analysis software (Mimics 11.0, Materialise US, MI). For the 100 and 400  $\text{mg}/\text{cm}^3$  density standards, three ROIs were measured in each of the three slices (Fig. 1(a) and (b)). For the 1000 and 1750  $\text{mg}/\text{cm}^3$  standards, a single ROI was identified in the center of each of the slices (Fig. 1(c) and (d)). The pixels in the boundary region of the standard were excluded to minimize edge artifacts. The implemented method used ROIs of 135 pixels for the 100 and 400  $\text{mg}/\text{cm}^3$  standards and 45 pixels for the 1000 and 1750  $\text{mg}/\text{cm}^3$  standards.

The mean HU for each ROI were converted to mineral density using the linear calibration equation determined as a function of the known mineral densities of the standards and the average of the HU obtained for each standard imaged seven times.

To assess the effect of imaging medium on calibrated density, ‘ground truth’ was defined by the linear relationship established between the known mineral density and the mean HU from the five replicated scans of the standards imaged in porcine soft tissue.

### *2.4 Statistical analysis*

The coefficient of variation for mineral density was determined for each standard for each of the seven replicate scans over the 19-week period and the overall value. The suitability of linear relationships used to convert HU to mineral density was determined using the coefficient of determination. A two-way repeated measures analysis of variance (ANOVA) was used to test the statistical hypothesis that there were no main effects on mean density values due to media and the standards. Bonferroni simultaneous post-hoc tests were performed to compare the mineral density values obtained when imaging the standards in water, and air with the control condition (imaging in porcine soft tissue). Statistical analyses were performed using a commercial software package (SigmaStat 3.5, Systat Software Inc., CA) and significance was set at  $p < 0.05$ .

## **3. Results**

Table 1 Mean (SD) Hounsfield Units (HU) and calibrated density (mg/cm<sup>3</sup>) and coefficients of variation in density (CV%) for four calibration standards imaged at seven different time points over a 19-week period

	Time							Overall
	1	2	3	4	5	6	7	
<b>100 mg/cm<sup>3</sup></b>								
HU	144.5 (3.01)	143.4 (0.66)	143.1 (0.83)	137.6 (2.72)	143.6 (1.16)	148.0 (5.27)	137.9 (1.04)	142.6 (4.13)
Density	91.29 (2.26)	90.51 (0.50)	90.27 (0.62)	86.14 (2.04)	90.64 (0.87)	93.95 (3.95)	86.35 (0.78)	89.88 (3.10)
CV(%)	2.47	0.55	0.69	2.37	0.96	4.21	0.91	3.45
<b>400 mg/cm<sup>3</sup></b>								
HU	551.6 (0.82)	545.8 (1.81)	553.1 (1.74)	567.6 (1.12)	559.7 (1.93)	561.7 (2.28)	566.1 (1.80)	557.9 (7.77)
Density	396.8 (0.62)	392.5 (1.36)	397.9 (1.31)	408.9 (0.84)	402.9 (1.45)	404.4 (1.71)	407.7 (1.35)	401.6 (5.83)
CV(%)	0.16	0.35	0.33	0.21	0.36	0.42	0.33	1.45
<b>1000 mg/cm<sup>3</sup></b>								
HU	1391.6 (5.52)	1371.9 (12.16)	1376.3 (11.46)	1383.3 (5.09)	1378.4 (6.97)	1379.7 (4.39)	1387.7 (6.13)	1381.3 (9.20)
Density	1027.2 (4.14)	1012.4 (9.12)	1015.7 (8.60)	1020.9 (3.82)	1017.2 (5.23)	1018.3 (3.29)	1024.3 (4.60)	1019.4 (6.90)
CV(%)	0.40	0.90	0.85	0.37	0.51	0.32	0.45	0.68
<b>1750 mg/cm<sup>3</sup></b>								
HU	2366.2 (6.45)	2367.3 (7.18)	2361.4 (7.54)	2315.9 (7.01)	2333.7 (2.89)	2329.9 (6.67)	2308.3 (5.48)	2340.4 (23.90)
Density	1758.5 (4.84)	1759.3 (5.39)	1754.9 (5.66)	1720.8 (5.26)	1734.1 (2.17)	1731.2 (5.01)	1715.0 (4.11)	1739.1 (17.90)
CV(%)	0.28	0.31	0.32	0.31	0.12	0.29	0.24	1.03

HU were consistent for each of the standards imaged in air at the seven time points (Table 1). The equation defining the relationship between HU acquired for each standard on seven occasions and the known mineral density ( $\rho$ ) of the calibration standards ( $HU = 1.333 \rho + 22.806$ ) was used to convert HU to density in mg/cm<sup>3</sup>. A linear fit between the calibrated and known mineral densities for the four standards was appropriate ( $r^2 = 0.9992$ ;  $y = 0.997x - 2.382$ ). The goodness of fit was comparable with the calibration equation determined using only the two standards with mineral densities in the range of trabecular bone ( $r^2 = 0.9990$ ;  $y = 1.054x - 21.464$ ), however the intercept differed by a factor of 10.

A linear relationship between calibrated density and the mineral density of the standards provided a good fit when imaging in soft tissue, water, and air ( $r^2 = 0.9994$ ,  $0.9995$  and  $0.9986$ , respectively). However, the effect of the imaging medium on the accuracy of the calibrated density differed depending upon the mineral density of the standard ( $p < 0.001$ , Fig. 4). Calibrated density was not different from the ‘ground truth’ when the standards were imaged in water ( $p = 0.08$  to  $1.00$ , Fig. 4, circles and triangles). For the standard with the lowest mineral density ( $100 \text{ mg/cm}^3$ ), the calibrated density was not significantly different from control values when imaged in water or

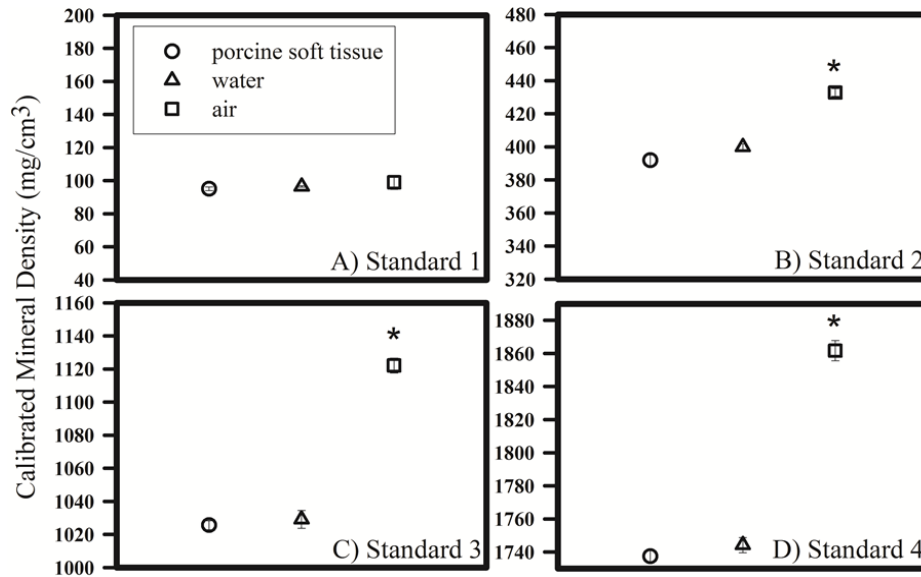


Fig. 4 Mean calibrated mineral density (error bars denote standard deviation) when standards are imaged 5 times in porcine soft tissue (control condition, circles), water (triangles), and air (squares) for: (a) Standard 1 ( $100 \text{ mg/cm}^3$ ), (b) Standard 2 ( $400 \text{ mg/cm}^3$ ), (c) Standard 3 ( $1000 \text{ mg/cm}^3$ ), and (d) Standard 4 ( $1750 \text{ mg/cm}^3$ ). Values significantly different from the control condition are indicated by an asterisk,  $p < 0.05$

air (Fig. 4(a)). In contrast, the calibrated densities were significantly higher than the control values when standards with higher mineral densities were imaged in air ( $p < 0.001$ , Fig. 4(b)-(d), circles and squares).

#### 4. Conclusions

We present a repeatable procedure for in vitro calibration of HU to densities typical of long bone. For the range of densities tested, error in the measure is negligible. In theory, the relationship between physical densities and HU is nonlinear. However, this work confirms that the linear relationship for conversion of HU to physical densities previously derived using density standards representative of trabecular bone is also appropriate for cortical bone. Furthermore, we provide experimental support for the practice of imaging the calibration standards in the same environment as the target bone.

We did not include bone specimens in our experiment. However, our results can be compared with recent work in which trabecular and cortical bone specimens were imaged in water using CT and the relationship between calibrated densities and ash weight was determined ( $r^2 = 0.997$ ) (Shileo *et al.* 2008). In the current study, the relationship between HU and calibrated mineral density for the standards imaged in water was ( $r^2 = 0.999$ , data not shown). The similarity in these results is noteworthy given that Schileo *et al.* (2008) based the calibration on a phantom representative of trabecular bone density. Thus, our study confirms that the linearity applies beyond the densities typical of trabecular bone and supports incorporation of these estimates of

cortical bone density in CT-based models of bone strength.

The consistency in the CV for the calibrated density of each standard indicates the hydroxyapatite is reasonably consistent throughout the volume and, therefore, there is no need to standardize the ROI location between one scan and another. As expected, the 100 mg/cm<sup>3</sup> standard has the greatest CV given that the standard deviation of the measure is normalized by the mean. Our results compare favorably with previously reported CV of 0.4 to 2.5% (Braillon 2002, Kalendar and Suess 1987, Steiger *et al.* 1990).

It should also be noted that, for the purposes of this study, the calibration was based solely on homogeneous standards with mineral densities within the range of trabecular and cortical bone tissue. Since the calibration was not based on a water equivalent standard, the calibration equations determined in this study do not have an intercept of zero, nor was the intercept forced to be zero. Therefore, this calibration is not suitable for studies focused on the quantification of specific soft tissue types or composition of soft tissues.

Our study is not without limitations. Calibration will be affected by the position of the standards in the field of view and each center will need to confirm the applicability of these results to the specific experimental set up. Schileo *et al.* (2008) however, found a comparable calibration equation (calibrated density = 0.7764 HU - 5.6148 in mg/cm<sup>3</sup>) using Brightspeed, CT scanner (GE Medical Systems, helical mode, slice spacing and reconstruction of 0.625 mm, 120 kV, 160 mAs, pixel dimensions 0.3125 × 0.3125 mm<sup>2</sup>) and three certified hydroxyapatite solution inserts of 50, 100 and 200 mg/cm<sup>3</sup> (European Spine Phantom) in water. It should also be noted that beam hardening corrections are scanner specific. The effect of the basic beam hardening correction algorithm included in all scan protocols acquired using our GE helical multi-slice CT scanner is observed in Fig. 2. The air condition represents the absence of beam hardening since there is no additional material in the path of the beam apart from the calibration standard. No further bone algorithm was used in our study. These results can not be generalized to protocols where other correction algorithms and/or CT scanners from other manufacturers are used.

Our study shows that conversion of HU to mineral density is highly repeatable for scans performed using identical imaging parameters and a General Electric Lightspeed Plus helical multi-slice CT scanner. To relate *ex vivo* CT data to *in vivo* conditions, it is important to scan a specimen and calibration standard in a soft tissue volume or in water, which most closely resembles the X-ray attenuation characteristics of soft tissue in the anatomical region of interest.

## Acknowledgements

Support from Dr. RW Sellens, Dr. JT Bryant, Degen Southmayd, Leone Ploeg and the CT Technologists, Kingston General Hospital, Queen's University, CFI, CIHR-New Emerging Teams (QNT-68721), CIHR Graduate Scholarship Master's Award, ORDCF, and NSERC (DG 311896) is gratefully acknowledged.

## References

- Araki, K. and Okano, T. (2011), "The effect of surrounding conditions on pixel value of cone beam computed tomography", *Clin. Oral Implants Res.*, doi: 10.1111/j.1600-0501.2011.02373.x.
- Au, A.G., Raso, V.J., Liggins, A.B. and Amirfazli, A. (2007), "Contribution of loading conditions and

- material properties to stress shielding near the tibial component of total knee replacements”, *J. Biomech.*, **40**, 1410-1416.
- Bessho, M., Ohnishi, I., Matsuyama, J., Matsumoto, T., Imai, K. and Nakamura, K. (2007), “Prediction of strength and strain of the proximal femur by a CT-based finite element method”, *J. Biomech.*, **40**, 1745-1753.
- Bouxssein, M.L. (2008), “Technology insight: noninvasive assessment of bone strength in osteoporosis”, *Nat. Clin. Pract. Rheumatol.*, **4**, 310–318.
- Braillon, P.M. (2002), “Quantitative computed tomography precision and accuracy for long-term follow-up of bone mineral density measurements”, *J. Clin. Densitom.*, **5**, 259-266.
- Brooks, R.A. and DiChiro, G. (1976), “Beam hardening in reconstructive tomography”, *Phys. Med. Biol.*, **21**, 390-398.
- Curry, J.D. (1988), “The effect of porosity and mineral content on the Young’s modulus of elasticity of compact bone”, *J. Biomech.*, **21**, 131-139.
- Genant, H.K., Cann, C.E., Ettinger, B. and Gordan, G. (1982), “Quantitative computed tomography of vertebral spongiosa: A sensitive method for detecting early bone loss after oophorectomy”, *Ann. Intern. Med.*, **97**, 699-706.
- Gong, H., Zhang, M., Fan, Y., Kwok, W.L. and Leung, P.C. (2012), “Relationships between femoral strength evaluated by nonlinear finite element analysis and BMD, material distribution and geometric morphology”, *Ann. Biomed. Eng.*, **40**, 1575-1585.
- Kalendar, W.A. and Suess, C. (1987), “A new calibration phantom for quantified computed tomography”, *Med. Phys.*, **14**, 863-866.
- Kalpakcioglu, B.B., Morshed, S., Engelke, K. and Genant, H.K. (2008) “Advanced imaging of bone macrostructure and microstructure in bone fragility and fracture repair”, *J. Bone Joint Surg. Am.*, **90**, 68-78.
- Kazakia, G.J. and Majumdar, S. (2006), “New imaging technologies in the diagnosis of osteoporosis”, *Rev. Endocr. Metab. Disord.*, **7**, 67-74.
- Pietruszczak, S., Gdela, K., Webber, C.E. and Inglis, D. (2007), “On the assessment of brittle-elastic cortical bone fracture in the distal radius”, *Eng. Frac. Mech.*, **74**, 1917-1927.
- Reggiani, B., Cristofolini, L., Varini, E. and Viceconti, M. (2006), “Predicting the subject-specific primary stability of cementless implants during pre-operative planning: preliminary validation of subject-specific finite-element models”, *J. Biomech.*, **40**, 2552-2558.
- Schileo, E., Dall’Ara, E., Taddei, F., Malandrino, A., Schotkamp, T., Baleani, M. and Viceconti, M. (2008), “An accurate estimation of bone density improves the accuracy of subject-specific finite element models”, *J. Biomech.*, **41**, 2483-2491.
- Steiger, P., Block, J.E., Steiger, S., Heuck, A.F., Friedlander, A., Ettinger, B., Harris, S.T., Gluer, C.C. and Genant, H.K. (1990), “Spinal bone mineral density measured with a quantitative CT: Effect of region of interest, vertebral level, and technique”, *Radiology*, **175**, 537-543.
- Unnikrishnan, G.U. and Morgan, E.F. (2011), “A new material mapping procedure for quantitative computed tomography-based, continuum finite element analyses of the vertebra”, *J. Biomech. Eng.*, **133**(7), 071001.
- Van Gompel, G., Van Slambrouck, K., Defrise, M., Batenburg, K.J., de Mey, J., Sijbers, J. and Nuyts, J. (2011), “Iterative correction of beam hardening artifacts in CT”, *Med. Phys.*, **38**, 36-49.